

Q-HyViT: Post-Training Quantization of Hybrid Vision Transformers with Bridge Block Reconstruction for IoT Systems

Jemin Lee[✉], Yongin Kwon[✉], Sihyeong Park[✉], Misun Yu[✉], Jeman Park[✉], and Hwanjun Song[✉]

Abstract—Recently, vision transformers (ViTs) have superseded convolutional neural networks in numerous applications, including classification, detection, and segmentation. However, the high computational requirements of ViTs hinder their widespread implementation. To address this issue, researchers have proposed efficient hybrid transformer architectures that combine convolutional and transformer layers with optimized attention computation of linear complexity. Additionally, post-training quantization has been proposed as a means of mitigating computational demands. For mobile devices, achieving optimal acceleration for ViTs necessitates the strategic integration of quantization techniques and efficient hybrid transformer structures. However, no prior investigation has applied quantization to efficient hybrid transformers. In this paper, we discover that applying existing post-training quantization (PTQ) methods for ViTs to efficient hybrid transformers leads to a drastic accuracy drop, attributed to the four following challenges: (i) highly dynamic ranges, (ii) zero-point overflow, (iii) diverse normalization, and (iv) limited model parameters (<5M). To overcome these challenges, we propose a new post-training quantization method, which is the first to quantize efficient hybrid ViTs (MobileViTv1, MobileViTv2, MobileFormer, EfficientFormerV1, EfficientFormerV2). We achieve a significant improvement of 17.73% for 8-bit and 29.75% for 6-bit on average, respectively, compared with existing PTQ methods (EasyQuant, FQ-ViT, PTQ4ViT, and RepQ-ViT). We plan to release our code at <https://gitlab.com/ones-ai/q-hyvit>.

Index Terms—Post-training quantization, vision transformer, model compression.

I. INTRODUCTION

RECENT advancements in quantization method have markedly enhanced the integration of federated learning and deep neural networks within the Internet of Things (IoT) domain [1]–[3], facilitating a significant leap towards more efficient computation and communication. These advancements enable IoT devices to engage in distributed, privacy-preserving machine learning, transforming them into highly intelligent

systems capable of real-time data analysis and autonomous decision-making. Through optimized hardware accelerators and communication-efficient protocols, quantization paves the way for the deployment of advanced AI models on edge devices, heralding a new era of intelligent, efficient, and autonomous IoT applications.

Meanwhile, thanks to self-attention that captures the global representation and shows better generalization with a low inductive bias, vision transformers (ViTs) have substituted convolutional neural networks (CNNs) in numerous applications, such as image classification, object detection, and instance segmentation [4], [5]. Despite the great success of ViT, the high computational requirement of ViTs still remains a significant impediment to their widespread implementation.

To democratize the use of ViT on resource-constrained devices, researchers have proposed a *hybrid* vision transformer architectures, which combine convolutional and transformer layers, such as MobileViTv1 [6]. They have also optimized attention computation to achieve linear complexity, such as MobileViTv2 [7]. Additionally, quantization techniques have been adopted for efficient architecture design, achieving model compression by reducing the precision of float values. Typically, the quantization techniques are categorized into two types: quantization-aware training (QAT) and post-training quantization (PTQ). While QAT offers advantages in preserving accuracy compared with PTQ, its adoption has been restricted due to privacy concerns, the resource-intensive and time-consuming nature of the re-training process, and the requisite expertise for hyperparameter tuning in architecture development [8]–[15].

In practical setup, PTQ methods have been more commonly employed due to their high applicability [8], [16]–[23]. PTQ enables the calibration of pre-trained models, utilizing only a small unlabeled dataset. PTQ for CNN models has been studied extensively, and recently, there has been a notable surge in interest regarding PTQ for ViTs. PTQ for ViTs shows its ability to maintain the accuracy of quantized models, effectively addressing varied activation ranges resulting from a non-linear function. However, these studies have solely focused on canonical transformer architectures, such as ViT [24], DeiT [25], and Swin Transformers [26].

For mobile devices, achieving optimal acceleration for ViTs necessitates the integration of quantization techniques and efficient transformer structures. However, there has been no

This work was supported by Institute of Information & communications Technology Planning & Evaluation (IITP) grant funded by the Korea government(MSIT) (No.RS-2023-00277060, Development of open edge AI SoC hardware and software platform) (Corresponding author: Hwanjun Song)

Jemin Lee, Yongin Kwon, Misun Yu, and Jeman Park are with the Artificial Intelligence Computing Research Laboratory, Electronics and Telecommunications Research Institute(ETRI), Republic of Korea (e-mail: {leejaymin, yongin.kwon, msyu, jeman}@etri.re.kr)

Sihyeong Park is with the SoC Platform Research Center, Korea Electronics Technology Institute(KETI), Republic of Korea (e-mail: sihyeong@keti.re.kr)

Hwanjun Song is with the Department of Industrial and Systems Engineering, KAIST, South Korea (e-mail: songhwanjun@kaist.ac.kr)

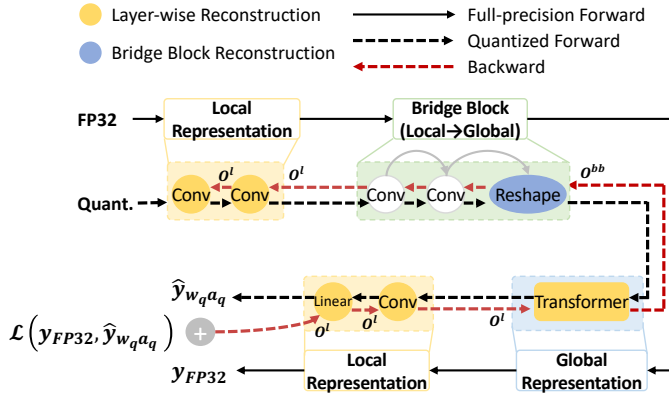


Fig. 1. Overall quantization process of Q-HyViT on the representative structure of hybrid vision transformers, including local, global, and bridge representation.

prior exploration into applying quantization to efficient hybrid transformers. While the existing PTQ can be directly applied to hybrid ViTs, this process is non-trivial due to the four key differences distinguishing them from the canonical ViTs: (i) *the highly dynamic activation range*, which complicates accuracy preservation using existing methodologies for pure ViTs; (ii) *the existence of bridge blocks*, which serves as connectors between convolution and transformer layers, introducing a disparity between local and global representations and the issue of zero-point overflow; (iii) *the diverse types of normalization techniques*, which are used in hybrid vision transformers; and (iv) *the small-sized models with less than 5 million parameters*, which lead to a substantial loss of robustness during quantization due to their limited number of parameters and minimal residual connections. Therefore, it is imperative to simultaneously adjust the granularity and scheme of both bridge and non-bridge layers, while also identifying the optimal scaling factors for quantization.

In this paper, we propose **Q-HyViT** in Figure 1, a tailored quantization approach for hybrid vision transformers aimed at minimizing quantization error. Q-HyViT integrates a novel *hybrid reconstruction* error minimization technique, which can determine the optimal scale factors, granularity (channel-wise or layer-wise), and quantization scheme (symmetric or asymmetric). Here, the reconstruction objective of each layer differs based on whether it is part of the bridge block¹ or not. To implement this technique in an integrated manner, we reuse the second-order term-based reconstruction error minimization method and extend it to incorporate the bridge block. To our knowledge, this is the *first* work that identifies the challenges of quantization for hybrid vision transformers and proposes a unified method to mitigate their errors in post-training quantization.

We conduct comprehensive experiments to compare Q-HyViT with existing open-source quantization methods, namely EasyQuant [27], FQ-ViT [28], PTQ4ViT [29], and RepQ-ViT [30], on the same hybrid ViTs. The experiments

¹The term “bridge block” literally refers to the transition part between convolution and transformer blocks. The precise constitution of this block slightly differs among hybrid ViT architectures.

use hybrid ViTs including MobileViTv1 [6], MobileViTv2 [7], MobileFormer [31], EfficientFormerV1 [32], and EfficientFormerV2 [33], which are representative variants of efficient ViTs.

The results demonstrate that our Q-HyViT performs considerably well across five types of hybrid ViTs and outperforms existing PTQ methods for pure ViTs (EasyQuant, PTQ4ViT, and RepQ-ViT) by a large margin (up to an average improvement of 17.73% for 8-bit and 29.75% for 6-bit). Particularly, we highlight that in *full* quantization setup where quantizing non-linear operations (softmax and normalization) is essential, Q-HyViT achieves state-of-the-art accuracy (an average improvement of 43.63% for 8-bit compared with FQ-ViT) on hybrid ViTs.

Our primary contributions are summarized below:

- We discover that quantization of hybrid ViTs presents four unique challenges: (i) the presence of highly dynamic activation ranges, (ii) zero-point overflow in the bridge block, (iii) diverse normalization, and (iv) a parameter count of less than 5 million.
- We propose a unified method called Q-HyViT, which is based on Hessian to adjust the granularity and scheme for bridge and non-bridge layers, while also determining the optimal scaling factors for quantization.
- We extend the existing PTQ methods to accommodate the five variants of efficient hybrid ViTs and directly compare them with our proposed Q-HyViT framework. Our experimental results reveal that Q-HyViT significantly outperforms state-of-the-art PTQ methods, including FQ-ViT, PTQ4ViT, and RepQ-ViT, in maintaining the accuracy of quantized hybrid ViTs.

II. RELATED WORK

Model architecture design and quantization techniques have received substantial attention in the context of efficient AI. We provide an overview of prior research endeavors on designing efficient ViT architectures and efficient quantization methods.

A. Efficient Computer Vision Architecture

To avoid heavy computation in CNNs, standard convolutions have been replaced with separable convolutions [34]. Separable convolutions have been widely used when designing light-weight CNNs including MobileNets [35]–[37], ShuffleNetv2 [38], and MNASNet [39], reducing the computational complexity of CNN operations. Despite the prevalence of these models, a major drawback of them is that they are spatially local and have higher inductive bias.

To expand model capacity while minimizing inductive bias, transformers [24] are employed for computer vision, where pure transformers are directly applied to process image patches as a sequence. Dosovitskiy *et al.* [24] showed that it performs better than recent CNN-based architectures on multiple image recognition benchmarks. Moreover, Touvron *et al.* [25] introduced a teacher-student strategy tailored for transformers, resulting in competitive convolution-free transformers trained solely on ImageNet data.

Even though pure ViT models achieve performance competitive to CNNs, the majority of them are computationally intensive. Recently, MobileViTv1 [6], MobileViTv2 [7], EfficientFormerV1 [32], EfficientFormerV2 [33], and MobileFormer [31] have been proposed for lightweight ViTs. Such hybrid ViTs show accuracy higher than light-weight CNNs (MobileNet series) with a comparable number of model parameters by incorporating a fusion of convolution and transformer layers.

B. Model Quantization

Quantization methods are categorized into two types: quantization-aware training (QAT) and post-training quantization (PTQ). Although QAT methods have successfully mitigated the accuracy degradation of quantized models by mapping from high-bit to low-bit precision [8]–[15], their widespread adoption has been hindered due to dependencies on re-training, the necessity of a complete dataset, and sophisticated hyper-parameter tuning.

Post-training quantization methods, which convert high-precision representation bits to low-precision bits without requiring re-training steps, have been extensively studied and widely adopted in practical scenarios [16], [18]–[23], [40], [41]. PTQ helps in the rapid deployment of CNN models on resource-constrained devices by addressing time-consuming and data privacy concerns. However, PTQ leads to significant accuracy degradation, particularly in low-precision representations, and prior research has mainly focused on `int8` quantization. As an effort to preserve the performance of a full-precision model, recent PTQ works [42]–[46] have suggested to reconstruction error minimization of each layer or block by adjusting the magnitude of weight rounding and searching optimal scaling factors.

Recently, quantization for ViTs has been studied [28]–[30], [47]–[49]. In efforts to minimize quantization errors, these research endeavors have taken into account the unique structure of ViTs, such as multi-head attention and layer normalization. However, they do not account for the distinctive characteristics of hybrid ViTs – the presence of bridge blocks and the utilization of diverse normalization techniques.

III. PRELIMINARY

A. Hybrid Vision Transformers and Bridge Blocks

To address the inefficiencies of canonical ViTs, hybrid ViTs have been proposed to combine convolutional operations with transformers. These aim to reduce model size without compromising on accuracy.

1) *Variants of Hybrid Vision Transformer*: From a broader perspective, recent hybrid vision transformers can be classified into three categories, namely MobileViTseries [6], [7], MobileFormer [31], and EfficientFormer series [32], [33].

MobileViT series: The fundamental principle underneath MobileViT’s design philosophy focuses on bringing together CNNs and ViTs in order to attain an optimal balance between efficiency and performance in the field of mobile vision tasks. By integrating transformer blocks within a CNN framework,

MobileViTv1 skillfully processes both local and global information, outperforming traditional models in parameter efficiency. The subsequent version, MobileViTv2, advances this approach by transforming the attention map from a quadratic $O(N^2)$ to linear $O(N)$ complexity, further enhancing computational efficiency.

Mobile-Former: The model excels by using MobileNet and Transformers together, bridging them with a bi-directional connector. This unique setup enables an effective exchange of local and global features, optimizing the model’s performance on mobile devices without compromising efficiency.

EfficientFormer series: This architecture differs from the use of MobileNet blocks and instead uses a convolutional stem followed by a pure transformer architecture specifically optimized for mobile usage. EfficientFormerV1 establishes a new benchmark by effectively tackling the common inefficiencies seen in ViTs, including channel size reduction and spatial downsampling. The EfficientFormerV2 model expands upon the existing framework by including a unified Feed Forward Network that incorporates depth-wise convolutions, a more condensed and deeper architecture, and a dual-path attention downsampling method.

2) *Bridge Blocks*: The Bridge Block varies in its exact location depending on each hybrid vision model, but fundamentally consists of operators that adjust dimensions to facilitate transitions between local and global representations. Specifically, for MobileViTv1 and MobileViTv2, it implies convolution and reshape operators to align the input dimensions of the Transformer. In the case of Mobile-Former, it refers to operators within the Mobile-Former Block that transition bi-directionally between local and global representations. For EfficientFormerV1, these are operators that convert meta-blocks from 4D to 3D. In the case of EfficientFormerV2, the bridge block consists of local and global transition operators present in the 3rd and 4th stages.

The term `bridge block` refers to the transitional part that connects both convolution and transformer blocks. This block’s precise configuration changes significantly among hybrid ViT structures. Table I lists detailed descriptions and operator names for each model. For MobileFormer, EfficientFormerV1, and EfficientFormerV2, the exact names of the operators that compose the bridge block vary slightly depending on the size of the model. The names shown in Table I are based on the smallest model size.

B. Hybrid Vision Transformer Quantization

Uniform quantization is a commonly used method to quantize neural networks, including convolution networks and transformers. As shown in Figure 1, quantization for hybrid vision transformers is divided into three parts: convolution, bridge block, and transformer. In uniform quantization, the weights and input activations are evenly quantized by each scale factor as:

$$\mathbf{x}_q = \mathcal{Q}(\mathbf{x}_r) = \text{clip}\left(\text{round}\left(\frac{\mathbf{x}_r}{\Delta_{\mathbf{x}}} + zp\right), \min, \max\right), \quad (1)$$

where \mathbf{x}_r is a real value (full precision) and \mathbf{x}_q is a quantized value. $\Delta_{\mathbf{x}}$ is a scaling factor that is calculated depending on the

TABLE I
DEFINITION AND PRECISE CONFIGURATION OF THE BRIDGE BLOCK WITHIN EACH HYBRID VISION TRANSFORMER

Model	Description	Detailed Operators	# of Bridge Blocks
MobileViTV1	Convolution and reshape operators to align the input dimensions of the Transformer	stages.2.1.convkxx.conv -> stages.2.1.conv1x1 stages.3.1.convkxx.conv -> stages.3.1.conv1x1 stages.4.1.convkxx.conv -> stages.4.1.conv1x1	3
MobileViTV2	Convolution and reshape operators to align the input dimensions of the Transformer	stages.2.1.convkxx.conv -> stages.2.1.conv1x1 stages.3.1.convkxx.conv -> stages.3.1.conv1x1 stages.4.1.convkxx.conv -> stages.4.1.conv1x1	3
Mobile-Former	It refers to operators within the Mobile-Former Block that transition bi-directionally between local and global representations	features.1.local.global.proj -> features.1.global.block.ffn.0 features.1.global.local.proj -> features.2.conv1.0 features.2.local.global.proj -> features.2.global.block.ffn.0 features.2.global.local.proj -> features.3.conv1.0 features.3.local.global.proj -> features.3.global.block.ffn.0 features.3.global.local.proj -> features.4.conv1.0 features.4.local.global.proj -> features.4.global.block.ffn.0 features.4.global.local.proj -> features.5.conv1.0 features.5.local.global.proj -> features.5.global.block.ffn.0 features.5.global.local.proj -> features.6.conv1.0 features.6.local.global.proj -> features.6.global.block.ffn.0 features.6.global.local.proj -> features.7.conv1.0 features.7.local.global.proj -> features.7.global.block.ffn.0 features.7.global.local.proj -> features.8.conv1.0 features.8.local.global.proj -> features.8.global.block.ffn.0	15
EfficientFormerV1	These are operators that convert feature maps from 4D Meta Block to 3D Meta Block	stages.2.blocks.5.mlp.fc2 -> stages.3.downsample.conv -> stages.3.blocks.0.mlp.fc1	1
EfficientFormerV2	The bridge block consists of local and global transition operators exist in the 3rd and 4th stages	stages.2.downsample.conv.conv -> stages.2.blocks.0.mlp.fc1.conv stages.3.downsample.attn.proj.conv -> stages.3.blocks.0.mlp.fc1.conv	2

quantization scheme: either asymmetric or symmetric. Also, z_p denotes the zero point and exists only when using the asymmetric scheme.

In the case of transformers, input data is first passed through a quantized embedding layer before entering the transformer blocks, which consist of a multi-head self-attention (MHSA) and a feed-forward network (FFN). The MHSA module computes queries \mathbf{Q} , keys \mathbf{K} , and values \mathbf{V} with their pre-trained weights \mathbf{W} and inputs \mathbf{X} .

In a given quantized multi-head self-attention layer (MHSA), the embedding matrix \mathbf{E} undergoes quantization to $\bar{\mathbf{E}}$ prior to being processed by linear projection layers. These projection layers are represented as $\bar{\mathbf{Q}} = \bar{\mathbf{w}}_Q \bar{\mathbf{E}}$, $\bar{\mathbf{K}} = \bar{\mathbf{w}}_K \bar{\mathbf{E}}$, and $\bar{\mathbf{V}} = \bar{\mathbf{w}}_V \bar{\mathbf{E}}$, where the quantized weights $\bar{\mathbf{w}}_Q$, $\bar{\mathbf{w}}_K$, and $\bar{\mathbf{w}}_V$ correspond to the \mathbf{Q} (Query), \mathbf{K} (Key), and \mathbf{V} (Value) projection layers, respectively.

The subsequent step in the multi-head self-attention operation involves the use of divided query, key, and value matrices: $\bar{\mathbf{Q}}_h = \bar{\mathbf{Q}}/h$, $\bar{\mathbf{K}}_h = \bar{\mathbf{K}}/h$, and $\bar{\mathbf{V}}_h = \bar{\mathbf{V}}/h$. Each of these matrices is divided by the number of heads (h) to facilitate the computation for each individual head. Hence, the multi-head self-attention operation is represented as follows:

$$\text{MHSA}(\bar{\mathbf{Q}}, \bar{\mathbf{K}}, \bar{\mathbf{V}}) = \text{concat}(\text{head}_i, \text{head}_{i+1}, \dots, \text{head}_n) \bar{\mathbf{W}}^O$$

$$\text{head}_i = \text{quant-attention}(\bar{\mathbf{Q}}_h, \bar{\mathbf{K}}_h, \bar{\mathbf{V}}_h) \quad (2)$$

In Eq. (2), the MHSA operation consolidates the results from each self-attention computation through concatenation followed by a linear projection to produce the final output.

The quantized weight matrix used for the linear projection of the concatenated output is $\bar{\mathbf{W}}^O$. By combining multiple heads, the multi-head self-attention enables the attention function to extract information from different representation sub-spaces, which would be unattainable with a single attention head.

The detailed calculation of *quant-attention* is described as

$$\text{quant-attention}(\bar{\mathbf{Q}}_h, \bar{\mathbf{K}}_h, \bar{\mathbf{V}}_h)$$

$$= \text{quant-softmax} \left(\frac{\bar{\mathbf{Q}}_h \times \bar{\mathbf{K}}_h^T}{\sqrt{d_k}} \right) \times \bar{\mathbf{V}}_h, \quad (3)$$

where d_k denotes the key vector dimension. In Eq. (3), the scaling factor ($\sqrt{d_k}$) is used to mitigate the issue of dot products becoming excessively large when d_k is large. This size increase can cause the Softmax function to produce very small gradients, which in turn could result in the well-known vanishing gradient issue. Thus, the scaling factor effectively reduces the magnitude of the dot product outcomes, averting this complication. After the MHSA layer, FFN takes a quantized output, which is concatenated from the results of MHSA as input.

A popular method to reduce quantization error in post-training is reconstruction error minimization [29], [42], [43], [48]. Previous works have focused on optimizing the task loss, $\mathcal{L} = \text{Cross Entropy}(\hat{\mathbf{y}}, \mathbf{y})$, where $\hat{\mathbf{y}}$ represents the quantized output and \mathbf{y} denotes the full precision output which is used as ground truth in PTQ. The expectation of the task loss is a function of network parameters \mathbf{w} , given by $\mathbb{E}[\mathcal{L}(\mathbf{x}, \mathbf{y}, \mathbf{w})]$, where \mathbf{x} denotes activation and \mathbf{y} denotes output. Quantization

introduces a small perturbation ϵ on the parameter $\hat{\mathbf{w}} = \mathbf{w} + \epsilon$. Following the prior works [29], [42], [43], [48], we calculate the influence of quantization on the task loss using Taylor series expansion as:

$$\mathbb{E}[\mathcal{L}(\mathbf{x}, \mathbf{y}, \hat{\mathbf{w}})] - \mathbb{E}[\mathcal{L}(\mathbf{x}, \mathbf{y}, \mathbf{w})] \approx \epsilon^\top \bar{\mathbf{g}}^{(\mathbf{w})} + \frac{1}{2} \epsilon^\top \bar{\mathbf{H}}^{(\mathbf{w})} \epsilon. \quad (4)$$

Since the weight perturbation ϵ is relatively small, a second-order term of Taylor expansion can be used. In this equation, $\bar{\mathbf{g}}^{(\mathbf{w})} = \mathbb{E}[\nabla_{\mathbf{w}} \mathcal{L}(\mathbf{x}, \mathbf{y}, \hat{\mathbf{w}})]$ is the gradient and can be ignored if the pre-trained model is well-converged. $\bar{\mathbf{H}}^{(\mathbf{w})} = \mathbb{E}[\nabla_{\mathbf{w}}^2 \mathcal{L}(\mathbf{x}, \mathbf{y}, \hat{\mathbf{w}})]$ is the Hessian matrix. The goal is to find a quantizer that includes optimal scaling factors or a rounding scheme to minimize the influence, given by $\min \mathbb{E}[\mathcal{L}(\mathbf{x}, \mathbf{y}, \hat{\mathbf{w}})] - \mathbb{E}[\mathcal{L}(\mathbf{x}, \mathbf{y}, \mathbf{w})]$. However, directly minimizing the task loss leads to overfitting problems due to small datasets during the calibration phase. Thus, the second-order term of the Taylor series (Eq.(4)) is used. Referring to BRECQ [43], to reduce computational cost, Eq.(4) is simplified by removing the gradient ($\bar{\mathbf{g}}^{(\mathbf{w})}$) and approximating $\epsilon = \Delta \mathbf{w}$ to the network output ($\Delta O = \hat{O} - O$) as:

$$\epsilon^\top \bar{\mathbf{H}}^{(x)} \epsilon \approx \Delta O^\top \bar{\mathbf{H}}^{(O)} \Delta O. \quad (5)$$

Referring to previous works [29], [42], [43], [48], MSE minimization based on the squared gradient that approximates the Hessian matrix captures the trend of the task loss more accurately than other metrics such as MSE, Cosine, and Pearson.

We adopt the methodology described in [27], [29], [48] to traverse a search space of scaling factors by linearly dividing the maximum-minimum range of \mathbf{w} and \mathbf{x} into n candidates as:

$$\left[\alpha \frac{MAX|\mathbf{w}_l|}{2^{k-1}}, \beta \frac{MAX|\mathbf{w}_l|}{2^{k-1}} \right] \quad (6)$$

$$\left[\alpha \frac{MAX|\mathbf{x}_l|}{2^{k-1}}, \beta \frac{MAX|\mathbf{x}_l|}{2^{k-1}} \right],$$

where α and β are utilized to control the number of candidates generated for scaling factors.

C. Challenges of Hybrid ViT Quantization

Here, we identify four critical challenges (C1–C4) that impede the quantization of hybrid ViTs and also explain why the current quantization method is insufficient.

1) *C1: Highly Dynamic Activation Range:* To keep the accuracy from dropping too much when activation ranges change much, the quantization granularity should be automatically changed based on how the channels are spread out in each layer. For layers that exhibit different ranges per channel, a scaling factor per channel could be chosen to preserve a specific layer [23]. Otherwise, channels exhibiting a narrow range might encounter the problem where all values are treated as zeros during the application of layer-wise quantization.

To this end, channel-wise granularity is good for highly dynamic activations across channels. When prioritizing accuracy preservation without considering latency, opting for a fine-grained granularity at the channel level could yield the highest accuracy. However, *this does not always hold true in the hybrid vision transformers*. Applying channel-wise quantization to every layer rather causes the scaling

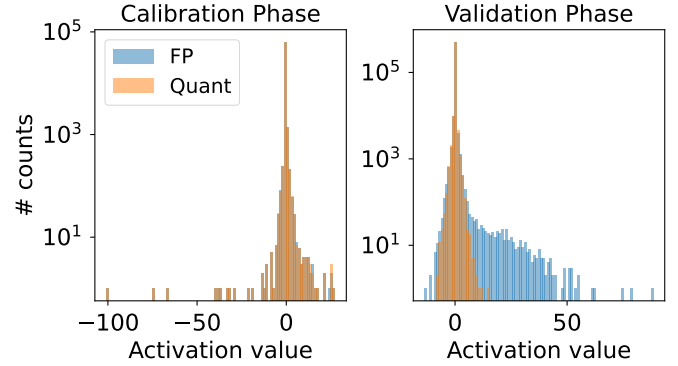


Fig. 2. Discrepancy in activation ranges between the calibration and validation datasets in 1st bridge block of MobileViTv2-100

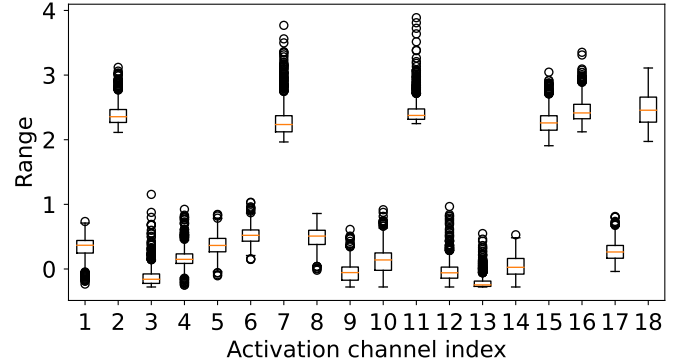


Fig. 3. Per activation channel ranges of convolution in bridge block of MobileViTv1-xxx

factors to overfit to small calibration data. This exacerbates the disparity between validation and calibration, resulting in a severe accuracy drop. Figure 2 shows the phenomenon in which scaling factors, determined channel-wise during the calibration phase, exhibit discrepancies during the validation phase. As a result, simply applying channel-wise granularity for quantization across all layers is problematic in hybrid ViTs. In layers where overfitting poses a concern, applying the scaling factor on a layer-wise basis can alleviate this issue. Therefore, determining the optimal granularity of the scaling factor is a critical consideration.

2) *C2: Zero-point Overflow in Bridge Block:* Uniform quantization comprises two types: asymmetric and symmetric quantization, each with its unique pros and cons. In many cases, asymmetric quantization shows better accuracy than symmetric quantization. However, we find out that *a severe accuracy drop occurs in the bridge block when using the asymmetric scheme or channel-wise granularity* due to highly dynamic activation ranges according to each channel and non-zero distribution.

This observation aligns with the prior discovery that the adoption of fine-grained granularity, such as channel-wise, does not always lead to a minimal quantization error.

As shown in Figure 3, the activation of the bridge block convolution shows a similar range for both the maximum and minimum values across all channels. This indicates that layer-

wise quantization does not lead to significant accuracy degradation. However, when applying channel-wise quantization to distributions such as the 2nd, 7th, 11th, and so on in Figure 3, where all values are greater than zero, overflow of the zero-point value for asymmetric quantization occurs (i.e., the zero-point value exceeded between -128 and 127). As shown in Figure 4, the clipped zero point is used, resulting in certain values being reconstructed as a single value.

As shown in Figures 5, 6, and 7, the issue of zero point overflow in activations within these bridge blocks is a phenomenon that exists across all bridge blocks in the MobileViT series (xxs, xs, and x). In addition, we observe that the impact of zero point overflow diminishes as our models increase in size. This is because the influence of zero point overflow decreases as the number of channels expands, as in the cases of 64 (xxs), 96 (xs), and 144 (s). Regardless of the model size, it is clear that clamping of specific values continues to occur in the bridge block. These issues manifest differently across models, necessitating an automated approach to choosing granularity and scheme.

Furthermore, for smaller models, we observe that the clamping issue associated with zero point overflow can be alleviated by transitioning from channel-wise quantization to layer-wise quantization, as demonstrated in Fig. 8. In the end, the reason why the zero point overflows are clamped is due to the following:

$$\begin{aligned}
 -128 &> q_{min} - \frac{r_{min}}{s} \\
 0 &> -\frac{r_{min}}{s} \\
 0 &< \frac{r_{min}}{s}
 \end{aligned} \tag{7}$$

In Eq. (7), q_{min} represents the minimum value of 8-bit quantization, which is -128 , s is the scaling factor, and r_{min} refers to the minimum value of the original activation. As shown in Eq. (7), since s is always a positive value, if r_{min} is greater than 0, the zero point exceeds the range of q_{min} and becomes clamped. Therefore, when quantizing on a per-channel basis, if activations are composed only of values greater than or equal to 0, it significantly causes a decrease in accuracy. To solve this issue, using layer-wise quantization takes into account the entire layer, including values less than or equal to 0 as r_{min} . Consequently, the zero-point value falls within the 8-bit range (-128 to 127).

3) *C3: Quantization with Diverse Normalizations: Hybrid vision transformers, unlike pure models such as CNN and ViT, employ different combinations of normalization techniques.* In the case of MobileViTv1, MobileFormer, EfficientFormerV1, and EfficientFormerV2, BatchNorm and LayerNorm are utilized, while MobileViTv2 uses BatchNorm and GroupNorm. To build a network as parameter-efficient as possible, various normalization techniques are employed in each hybrid vision transformer. However, a method to quantize all the normalization techniques used has yet to be proposed. In detail, unlike BatchNorm, the computation of LayerNorm, GroupNorm, and InstanceNorm requires dynamic computation to determine the mean and variance. When dynamic operations are handled in a floating point, additional data movement occurs in off-

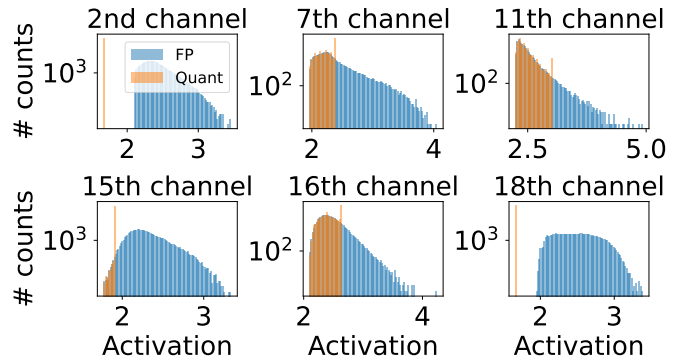


Fig. 4. The selected problematic activation channels of convolution in bridge block of MobileViTv1-xxs due to overflow of zero point when using the channel-wise manner and asymmetric scheme

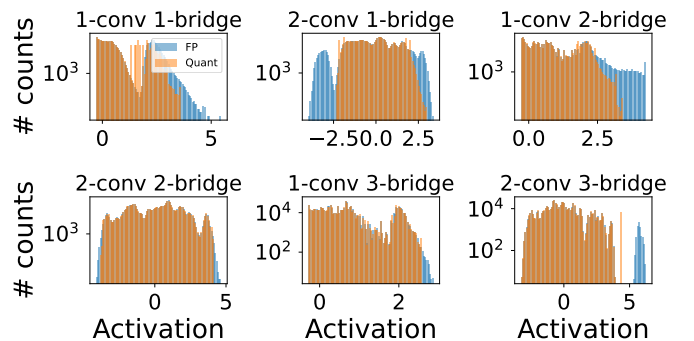


Fig. 5. A histogram depicting the overlap between quantized values (blue) and real values (orange) for six activation layers in the 1st, 2nd, and 3rd bridge blocks of the MobileViTv1-xxs model

chip memory. Therefore, to minimize the inference latency, the normalization should be quantized so that as many dynamic operations as possible can be processed in the integer domain.

4) *C4: Sub-5M Parameter Models:* Compared to heavy CNN models such as ResNet and VGG series, lightweight models with a relatively small number of parameters and few residual connections are more susceptible to the quantization process. *This vulnerability is particularly pronounced in models that have fewer than 5M parameters, where the quantization error is significantly higher in hybrid vision transformers.* As previously mentioned, using an asymmetric scheme for an activation distribution with a minimum value of 0 or greater can lead to force clamping due to the zero point overflow problem, making the accuracy more sensitive to the quantization granularity and scheme.

IV. METHODOLOGY

Addressing the four identified challenges (C1–C4), we design Q-HyViT, a precise post-training quantization framework specifically tailored for hybrid ViTs. It automatically identifies optimal layer-wise strategies – choosing granularity (channel-wise or layer-wise) for C1, C2, and C4, quantization scheme (symmetric or asymmetric) for C2 and C4, and quantization scaling factor for C3 and C4. This is achieved by leveraging the proposed hybrid reconstruction error minimization method.

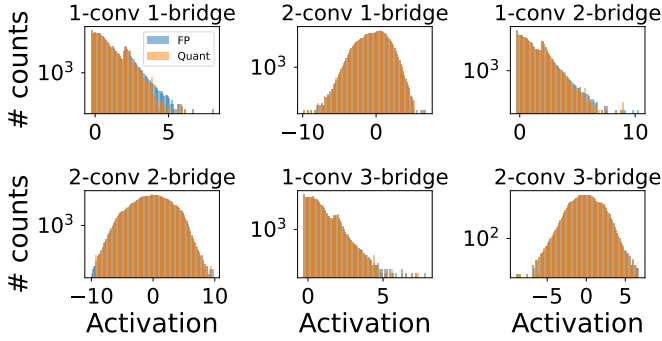


Fig. 6. A histogram depicting the overlap between quantized values (blue) and real values (orange) for six activation layers in the 1st, 2nd, and 3rd bridge blocks of the MobileViTv1-xs model

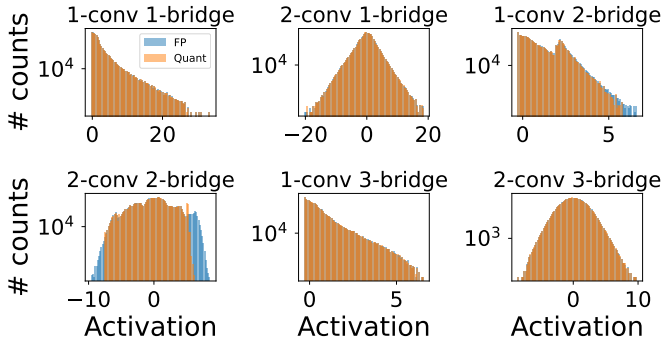


Fig. 7. A histogram depicting the overlap between quantized values (blue) and real values (orange) for six activation layers in the 1st, 2nd, and 3rd bridge blocks of the MobileViTv1-s model

A. Hybrid Reconstruction Error Minimization

Previous post-training quantization methods for ViTs have typically aimed to optimize the quantization task loss, which is achieved through the utilization of reconstruction error minimization, relying on second-order metrics to assess potential scaling factors for quantization. Furthermore, these methods incorporate a weight-rounding mechanism to enhance the overall quantization process. However, faced with the challenges specific to hybrid vision transformers, they become less effective in dealing with *bridge blocks*, which contain a gap between local and global representation, and *high dynamic activation ranges* resulting from the mixed structure of CNN and transformer.

To address these issues, Q-HyViT introduces *hybrid reconstruction error minimization*, the schematic of which is illustrated in Figure 1. As depicted in Figure 1, the Hybrid ViT architecture is divided into three distinct blocks for quantization: local, global, and bridge. The local blocks primarily consist of several convolutional layers, with the output from these layers denoted as \hat{O}^l . To mitigate overfitting issues on the small calibration dataset and alleviate high computational demands, the reconstruction error for each layer's output is calculated.

The global block, representing the transformer, computes the reconstruction error in a manner similar to the local block, using \hat{O}^l as a reference. The bridge block serves as a

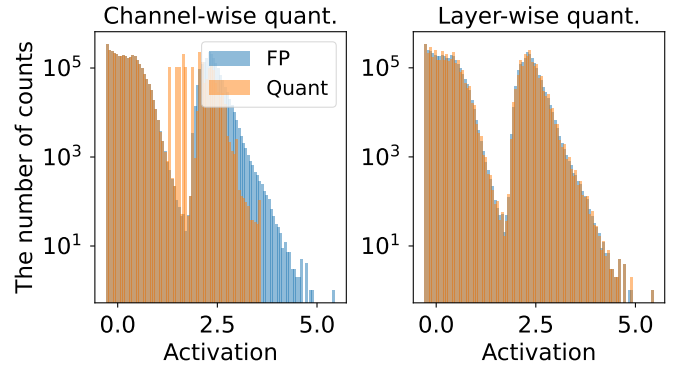


Fig. 8. An overlapping histogram of quantized values (blue) and real values (orange) in the activation of for 1st bridge block of MobileViTv1-xxs: (left) channel-wise quantization (right) layer-wise quantization

transitional operator facilitating the integration between local and global processing. Specific operations within this block may vary slightly across different models. To alleviate issues related to the highly dynamic activation range within the bridge block, the reconstruction error is calculated based on the output of this block, denoted as \hat{O}^{bb} , taking into account all dependencies within the block to optimize the process.

The model's quantization process encompasses both forward (illustrated by solid and dashed lines in Figure 1) and backward (illustrated by dashed red lines in Figure 1) passes. The diagram outlines the computation of a loss function \mathcal{L} , which is likely designed to measure the discrepancy between the full-precision output y_{FP32} and the quantized output $\hat{y}_{w_q a_q}$. This loss function is utilized to update the model parameters during calibration to minimize quantization errors.

The proposed method distinguishes the reconstruction strategy based on whether a given layer is part of the bridge block or not. It then determines the appropriate granularity and quantization scheme for each layer during post-training quantization. The reconstruction objective (O^{bb}) of the hybrid approach can be represented as:

$$O^{bb} = \begin{cases} \mathbf{w}_n^{bb} \mathbf{w}_{n-1}^{bb} \cdots \mathbf{w}_1^{bb} \mathbf{x}^{bb}, & \text{if a layer is in a bridge block} \\ \mathbf{w}^\ell \mathbf{x}^\ell, & \text{otherwise } bb \text{ is equal to } \ell \end{cases} \quad (8)$$

In Eq. (8), O^{bb} is determined to be either a single layer or multiple layers based on the presence of a bridge block. When a layer is part of the bridge block, the objective encompasses all the preceding layers within that bridge block.

Moreover, our hybrid reconstruction not only enables hybrid ViTs to achieve minimal quantization errors, but also determines quantization granularity and scheme automatically for each layer, using the hybrid reconstruction equation, guided

by the reconstruction objective:

$$\min_{\Delta, g, s} \mathbb{E} \left[\Delta O^{(bb), \tau}, \mathbf{H}^{O^{(bb)}} \Delta O^{(bb)} \right] \approx$$

$$\min_{\Delta, g, s} \mathbb{E} \left[\Delta O^{(bb), \tau}, \text{diag} \left(\left(\frac{\partial L}{\partial O_1^{(bb)}} \right)^2, \dots, \left(\frac{\partial L}{\partial O_{|O^{(bb)}}} \right)^2 \right) \Delta O^{(bb)} \right], \quad (9)$$

where bb is $\in [BridgeBlock, a\ layer]$. In Eq. (9), $\Delta O^{(bb)}$ is the difference between the quantization outputs before and after. $O_n^{(bb)}$ indicates the n -th element of O^{bb} . The range of n is from 1 to $O_{|O^{(bb)}}|$. As a result, we optimize the optimal scaling factor ($\Delta \in [1, 100]$), granularity ($g \in [layer, channel]$), and scheme ($s \in [asymmetric, symmetric]$) through hybrid reconstruction error minimization.

B. Implementing Q-HyViT: From Calibration to Optimization

The proposed Q-HyViT method, as outlined in Algorithm 1, leverages hybrid reconstruction to determine optimal scaling factors, granularity, and scheme. Thus, it effectively diminishes quantization errors in hybrid ViTs.

The algorithm 1, similar to PTQ methods, can be divided into two primary stages: calibration and quantization optimization. These stages are organized around three outermost while loops.

Throughout the calibration stage, Q-HyViT computes the output and gradient of each bridge block and layer via forward and backward propagation. These operations correspond to the first and second while loops in Algorithm 1 (*lines 1–11*). Specifically, the first while loop executes the model without quantization to calculate and store $\mathbf{y}^{(fp32)}$ and the intermediate results O_i^{bb} of the layers. The second while loop performs the default quantization layer (min-max scaling) or bridge blockwise, then computes the loss based on the difference from the outputs of the first loop to perform backpropagation, storing the outputs and gradients of each layer and bridge block.

The third while loop represents the optimization of quantization across all hybrid transformer layers by minimizing reconstruction error (*lines 12–18*). As mentioned, in hybrid ViTs, the dynamic activation range varies widely, necessitating automated adjustment methods. From this perspective, this approach minimizes quantization errors to enhance the second-order metric and ultimately leads to more accurate models.

To provide a more intuitive understanding, we describe how Algorithm 1 addresses each challenge we identified: (1) *a highly dynamic activation range* (refer to §III-C1) is addressed in the third loop of Algorithm 1, which identifies optimal granularity (either channel-wise or layer-wise). As mentioned previously, an indiscriminate choice of channel granularity can lead to overfitting with a small calibration dataset; hence, channel-wise granularity is selected only when necessary, considering the activation range. (2) *zero-point overflow in bridge blocks* (See to §III-C2) is also resolved by optimal granularity selection and further alleviated by optimally choosing the quantization scheme. Zero-point overflow, a problem of exceeding the min-max range, can be mitigated by adjusting

Algorithm 1: The tuning process of Q-HyViT

Input: A hybrid vision transformer model and a few images for calibration;

Output: Optimal scaling factors (Δ^*) scheme (s) and granularity (g);

```

1 while a layer( $\ell$ ) is not the end of layer do
  /* full-precision outputs on each layer
   including final layer ( $\mathbf{y}^{(fp32)}$ ) */
2  $O_\ell^{bb} \leftarrow$  forward propagation ( $\mathbf{w}_\ell \mathbf{x}_\ell$ )
3 end
4 while a layer( $\ell$ ) is not the end of layer do
5   if a layer( $\ell$ ) in a Bridge Block then
6     | Backward propagation to get  $\frac{\partial \mathcal{L}}{\partial O^{bb}}$ 
7   end
8   else
9     | Backward propagation to get  $\frac{\partial \mathcal{L}}{\partial O^\ell}$ 
10  end
11 end
12 while a layer( $\ell$ ) is not the end of layer do
  /* initialize scaling factors */
13  $\Delta_{\mathbf{w}_\ell^{bb}}^*, \Delta_{\mathbf{x}_\ell^{bb}}^* \leftarrow \frac{\text{MAX}(|\mathbf{w}_\ell^{bb}|)}{2^k}, \frac{\text{MAX}(|\mathbf{x}_\ell^{bb}|)}{2^k}$ 
  /* Generate candidates for scaling
   factors */
14  $\Delta_{\mathbf{w}_\ell^{bb}}, \Delta_{\mathbf{x}_\ell^{bb}} \leftarrow$  Eq. (6)
15 while Three iterations do
  /* Determine granularity, scheme,
   scaling factors */
16  $g, s, \Delta_{\mathbf{w}_\ell^{bb}}^*, \Delta_{\mathbf{x}_\ell^{bb}}^* \leftarrow$  Eq. (9)
17 end
18 end
19 return  $\Delta^*, g, s$ 

```

the scheme to symmetric or tuning the min-max values through granularity. These optimal choices are automatically made to minimize the reconstruction error. (3) *diverse normalization* (refer to §III-C3) is directly addressed by the proposed implementation of hybrid reconstruction error minimization. The proposed algorithm is implemented not only for layer normalization, but also extends to group and batch normalization, optimizing scaling for each. (4) *Quantization of sub-5M parameter models* inevitably leads to accuracy loss due to the lack of redundant parameters (See to §III-C4). Therefore, all the proposed components outlined in Algorithm 1 are employed to ensure that our quantization preserves accuracy as much as possible. However, the quantization of extremely small-sized models remains a difficult challenge, necessitating further exploration of various approaches.

V. EXPERIMENTS

We conduct extensive comparisons of Q-HyViT against various existing quantization methods. As discussed previously, there is no comprehensive method to quantize the hybrid vision transformers. Therefore we directly implemented the following open-sourced state-of-the-art quantization algorithms for pure vision transformers, namely EasyQuant [27], FQ-ViT [28], PTQ4ViT [29], and RepQ-ViT [30] and then applied them on five hybrid vision transformer architectures.

TABLE II
A COMPARISON OF THREE POST-TRAINING QUANTIZATION METHODS FOR IMAGE CLASSIFICATION ON IMAGENET-1K USING FIVE HYBRID ViT ARCHITECTURES AND BIT-WIDTHS. IN QUANTIZED MODELS, SOFTMAX AND LAYER-NORM REMAIN UNDER FLOATING-POINT.

Model	# Params.	Type	FP32	EasyQuant [27]		PTQ4ViT [29]		RepQ-ViT [30]		Ours	
				W8A8	W6A6	W8A8	W6A6	W8A8	W6A6	W8A8	W6A6
MobileViTv1-xxs	1.3M	Hybrid	69.0	36.13	10.17	37.75	30.80	1.85	1.38	68.20	66.33
MobileViTv1-xs	2.3M	Hybrid	74.8	73.16	55.22	65.52	62.56	41.96	27.29	74.31	73.44
MobileViTv1-s	5.6M	Hybrid	78.4	74.21	42.70	68.19	65.07	59.01	56.61	77.92	77.18
MobileViTv2-050	1.4M	Hybrid	70.2	66.80	11.58	39.39	45.38	26.60	27.89	69.89	69.07
MobileViTv2-075	2.8M	Hybrid	75.6	62.91	2.54	65.54	65.85	55.52	40.61	75.29	74.58
MobileViTv2-100	4.9M	Hybrid	78.1	69.34	0.12	51.02	47.27	40.85	26.07	77.63	77.11
MobileViTv2-125	7.5M	Hybrid	79.6	77.31	4.56	67.39	59.39	41.65	30.43	79.31	77.03
MobileViTv2-150	10.6M	Hybrid	80.4	75.83	10.39	68.61	67.58	62.12	58.71	80.09	79.97
MobileViTv2-175	14.3M	Hybrid	80.8	79.93	47.22	72.30	71.78	63.52	62.89	80.63	80.45
MobileViTv2-200	18.5M	Hybrid	81.2	80.04	57.32	75.50	74.65	64.65	62.15	80.94	80.76
Mobile-Former-26m	3.2M	Hybrid	64.0	28.95	0.12	58.27	47.25	0.11	0.16	61.78	51.06
Mobile-Former-52m	3.5M	Hybrid	68.7	62.16	17.29	67.32	62.01	1.12	1.00	67.79	62.65
Mobile-Former-96m	4.6M	Hybrid	72.8	53.31	33.68	71.32	64.72	0.40	0.25	71.60	64.21
Mobile-Former-151m	7.6M	Hybrid	75.2	4.98	3.49	73.86	68.16	0.11	0.12	74.30	68.44
Mobile-Former-214m	9.4M	Hybrid	76.7	72.79	28.32	75.01	68.24	0.13	0.14	75.76	69.34
Mobile-Former-294m	11.4	Hybrid	77.9	74.15	59.55	76.96	74.48	1.05	0.58	76.93	74.6
Mobile-Former-506m	14.0M	Hybrid	79.3	78.01	67.14	75.44	70.13	0.19	0.26	75.60	74.67
EfficientFormerV1-L1	12.3M	MetaBlock	80.2	78.24	58.83	80.11	79.8	80.36	78.55	80.15	77.25
EfficientFormerV1-L3	31.3M	MetaBlock	82.4	82.39	80.38	82.39	82.36	82.41	82.29	82.46	82.18
EfficientFormerV1-L7	82.1M	MetaBlock	83.3	83.24	81.89	83.34	83.16	83.28	83.03	83.31	83.12
EfficientFormerV2-S0	3.5M	Hybrid	76.2	68.21	41.24	68.40	41.26	40.02	37.11	74.69	74.18
EfficientFormerV2-S1	6.1M	Hybrid	79.7	66.42	2.69	73.44	73.34	58.30	53.06	77.56	77.54
EfficientFormerV2-S2	12.6M	Hybrid	82.0	71.80	7.02	79.85	79.39	70.39	70.37	80.62	80.30
EfficientFormerV2-L	26.1M	Hybrid	83.5	80.34	3.34	82.46	82.22	76.72	74.33	82.80	82.71

TABLE III
FULLY QUANTIZED ACCURACY OF HYBRID VISION TRANSFORMER ARCHITECTURES.

Model	# Params.	Type	FP32	FQ-ViT	Ours
MobileViTv1-xxs (MVv1-xxs)	1.3M	Hybrid	68.91	0.1	67.20
MobileViTv1-xs (MVv1-xs)	2.3M	Hybrid	74.64	62.2	73.89
MobileViTv1-s (MVv1-s)	5.6M	Hybrid	78.31	74.94	77.72
MobileViTv2-050 (MVv2-050)	1.4M	Hybrid	70.16	5.00	68.73
MobileViTv2-075 (MVv2-075)	2.8M	Hybrid	75.62	34.60	74.36
MobileViTv2-100 (MVv2-100)	4.3M	Hybrid	78.09	0.40	77.13

A. Implementation Details

For a fair comparison, we maintained most configurations consistent with EasyQuant, PTQ4ViT, RepQ-ViT, and FQ-ViT. Specifically, our settings vary depending on whether the model is fully quantized or not. Additionally, the five hybrid vision transformer models were referred to as the official models.

1) *Model Download*: Except for Mobile-Former, the other four hybrid models leverage the `timm` framework². Meanwhile, Mobile-Former is built upon the implementation by AABoys³. We successfully replicated the original accuracy using open-source codes under FP32 precision.

2) *Settings for EasyQuant and PTQ4ViT*: In EasyQuant, we quantized all operators, including fully-connected layers and matrix multiplications. To obtain the optimal scaling factors, we employed a search algorithm based on cosine distance. The search space was derived from $\alpha = 0.5$ and $\beta = 1.2$.

In PTQ4ViT, we adjusted the hyperparameters to $\alpha = 0$ and $\beta = 1.2$. Similar to PTQ4ViT, this study adopted the parallel

quantization method to prevent a significant accuracy drop caused by small datasets.

In both cases, we selected a sample of 32 images from the training dataset during the calibration process.

3) *Settings for RepQ-ViT*: To reproduce the results, we used the default settings from the code published by RepQ-ViT. During calibration, RepQ-ViT uses the percentile [50]. For quantization, we applied an asymmetric method with channel-wise granularity for weights and layer-wise granularity for activations. We used the default setting of 32 sample images for calibration.

4) *Settings for FQ-ViT*: Essentially, we performed symmetric quantization on a per-channel basis for weights and asymmetric quantization on a per-layer basis for activations. To ensure a fair comparison, we set the quantization for the weights to the minimum and maximum values. The hyperparameter K in the power of two factor remained unchanged. For the calibration process, we selected a sample of 1,000 images.

5) *Settings for Q-HyViT*: We quantized all the weights and inputs for the fully connected layers, including the first projection layer and the last head layer. Additionally, the two input matrices for the matrix multiplications in the self-attention modules were quantized. The inputs of the softmax and normalization layers were also quantized, which was consistent with FQ-ViT. We used 32 images for calibration, and unoptimized scaling factors were initialized with minimum and maximum values.

²<https://github.com/huggingface/pytorch-image-models>

³<https://github.com/AABoys/MobileFormer>

B. Accuracy Evaluation

We selected MobileViTv1 [6], MobileViTv2 [7], MobileFormer [31], EfficientFormerV1 [32], and EfficientFormerV2 [33] as representative hybrid vision transformer architectures.

1) *Results with Partial Quantization.*: Table II shows quantization results on hybrid ViT architectures with varying model sizes, in terms of 8-bit and 6-bit quantization, where softmax and layer-norm remain under floating-point.

Upon analyzing Table II, it is clear that prior studies have observed a significant drop in accuracy, even when using 8-bit quantization, in hybrid vision transformers. PTQ4ViT and EasyQuant perform fairly well by exploring scaling factors for each layer using Hessian and Cosine similarity to minimize reconstruction error when the model size is large. However, for models with fewer than 5M parameters, such as extremely lightweight models, existing quantization methods inadequately address dynamic activation changes. This leads to significant accuracy degradation, even in 8-bit settings. In the case of RepQ-ViT, accuracy is well preserved when the model size is large, but when the model size is reduced to less than 5M, there is a significant drop in accuracy. The RepQ-ViT model lacks the ability to include weight adjustment via a reconstruction approach, hence inadequately addressing the complex activations that occur in hybrid vision transformers. Therefore, it shows lower accuracy compared with prior works that used reconstruction methods (PTQ4ViT and Q-HyViT). Particularly, in MobileFormer, the granularity adjustment proposed by RepQ-ViT through reparameterization fails to accommodate the changes in activation that occur in hybrid vision transformers, resulting in the most significant drop in accuracy.

In contrast, our Q-HyViT achieves less than 1% accuracy drop with 8-bit quantization on the sub-5M models including xxs, xs, 050, 075, 100, 26m, 52m, 96m, and S0. In summary, Q-HyViT exhibits average improvements of 9.54% and 7.09% over EasyQuant and PTQ4ViT, respectively, with an 8-bit setting. Under the 6-bit setup, the improvements reach 43.39% and 8.65%, respectively.

Specifically, MobileViTv2 shows more accuracy drop than MobileViTv1 at the same model size, potentially due to its use of linear attention in self-attention computation, which results in fewer attention maps and lower resilience after post-softmax values. In the case of EfficientFormerV1, there is no significant difference between the conventional method and the proposed method. The reason for this is that convolution and transformer layers in the meta block are not used in a hybrid manner. Furthermore, we observe that larger hybrid vision transformers are less sensitive to low-bit quantization (6-bit), as evidenced by the accuracy drops of MobileViTv1-xxs, MobileViTv1-xs, and MobileViTv1-s, which are 2.67%, 1.36%, and 1.22%, respectively. This pattern is also consistent in MobileViTv2, MobileFormer, EfficientFormerV1, and EfficientFormerV2. This phenomenon is attributed to larger networks that have more weights and generate more activations, making them more resilient to perturbations caused by quantization.

2) *Results with Full Quantization.*: Previous studies [27], [29], [47], [48] have refrained from quantizing softmax and

TABLE IV

ABLATION STUDY ON HYBRID RECONSTRUCTION ERROR MINIMIZATION, WHERE ✓ DENOTES THAT THE COMPONENT IS CONSIDERED. WHEN ALL COMPONENTS ARE DISABLED, THE ACCURACY RESULTS ARE IDENTICAL TO THOSE OF PTQ4ViT.

Model Name	Scaling Factor (C3,C4)	Granularity (C1,C2,C4)	Scheme (C2,C4)	Top1 Accuracy
MobileViTv1-xxs	✗	✗	✗	37.75
	✓	✗	✗	44.37
	✓	✓	✗	59.50
	✓	✓	✓	68.20
MobileViTv1-xs	✗	✗	✗	65.52
	✓	✗	✗	69.12
	✓	✓	✗	72.00
	✓	✓	✓	74.31
MobileViTv1-s	✗	✗	✗	68.19
	✓	✗	✗	73.02
	✓	✓	✗	77.01
	✓	✓	✓	77.92
MobileViTv2-050	✗	✗	✗	39.39
	✓	✗	✗	49.62
	✓	✓	✗	69.89
	✓	✓	✓	69.89
MobileViTv2-075	✗	✗	✗	65.54
	✓	✗	✗	67.24
	✓	✓	✗	75.29
	✓	✓	✓	75.29
MobileViTv2-100	✗	✗	✗	51.02
	✓	✗	✗	68.18
	✓	✓	✗	77.63
	✓	✓	✓	77.63
MobileViTv2-125	✗	✗	✗	67.39
	✓	✗	✗	75.39
	✓	✓	✗	79.31
	✓	✓	✓	79.31
MobileViTv2-150	✗	✗	✗	68.61
	✓	✗	✗	75.88
	✓	✓	✗	80.09
	✓	✓	✓	80.09
MobileViTv2-175	✗	✗	✗	72.30
	✓	✗	✗	76.81
	✓	✓	✗	80.63
	✓	✓	✓	80.63
MobileViTv2-200	✗	✗	✗	75.50
	✓	✗	✗	77.91
	✓	✓	✗	80.94
	✓	✓	✓	80.94

layer normalization operations due to their smaller computational demand compared to matrix multiplication in terms of total FLOPs. Moreover, straightforward quantization of such non-linear functions may result in considerable accuracy degradation. Nonetheless, integer-only quantization [51] is important especially for edge and mobile devices. This is due to the fact that softmax operation and layer normalization require dequantization for their computation in floating-point, as well as data movement involved in off-chip memory. Thus, a fully quantized approach is necessary to alleviate significant hardware design challenges that arise from reducing off-chip level data transfer.

In line with previous research [28], we apply a fully quantized approach, FQ-ViT, to hybrid ViTs, as summarized in Table III. Note that FQ-ViT shows very poor accuracy in MobileViTv1-xxs due to its use of an asymmetric scheme with zero points, which fails to handle the high variation of activation range by adjusting quantization granularity. As

the size of the model increases, along with an increase in the number of channels, the effect of zero point overflow on accuracy becomes less significant compared to smaller models.

Furthermore, in the case of MobileViTv2, group normalization is utilized instead of batch and layer norms, causing the existing L2 norm-based scaling factor exploration to function inaccurately. Our study addresses these issues and achieves an average of 43.63% accuracy improvement over FQ-ViT.

C. Impact of Calibration Sample Size on Model Accuracy

As listed in Table II (partial quantization) and Table III (full quantization), the accuracy of each model varies depending on whether the softmax and layer-norm are quantized and the number of images utilized during the calibration phase. For a fair comparison with EasyQuant and PTQ4ViT in Table II, 32 images were used to obtain the results. In the case of FQ-ViT, the calibration utilized the 1,000 images referenced in the original paper. When increasing the number of images for calibration in partial quantization from 32 to 128, there are no significant differences in accuracy, as listed in Table V.

TABLE V
QUANTIZATION RESULTS UNDER DIFFERENT NUMBERS OF CALIBRATION IMAGES. PARTIAL MEANS THAT SOFTMAX AND LAYER-NORM REMAIN IN FLOATING-POINT, WHILE FULL MEANS THAT THEIR OPERATORS ARE QUANTIZED

Model	Quant.	# of images	Accuracy
MobileViTv1-xxs	Partial	32	68.20
	Partial	128	68.18
	Full	500	67.16
	Full	1,000	67.20
MobileViTv1-xs	Partial	32	74.31
	Partial	128	74.25
	Full	500	73.82
	Full	1,000	73.89
MobileViTv2-s	Partial	32	77.92
	Partial	128	77.67
	Full	500	77.69
	Full	1,000	77.72
MobileViTv2-050	Partial	32	69.89
	Partial	128	69.89
	Full	500	68.52
	Full	1,000	68.73
MobileViTv2-075	Partial	32	75.29
	Partial	128	75.32
	Full	500	74.26
	Full	1,000	74.36
MobileViTv2-100	Partial	32	77.63
	Partial	128	77.75
	Full	500	77.19
	Full	1,000	77.13

D. Running time of quantization methods

To compare the running times among various quantization methods, we measured the running times for five models using one A100-80G GPU for each quantization method. The results are shown in Figure 9, where the proposed Q-HyViT takes the longest with an average of 523 seconds, and the RepQ-ViT method takes the shortest time with an average

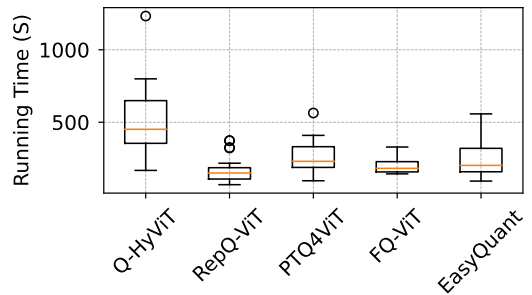


Fig. 9. Running time of quantization methods

of 159 seconds. These differences are influenced by whether the method performs reconstruction and the number of images used for calibration during quantization. Reconstruction methods, such as EasyQuant, PTQ4ViT, and the proposed Q-HyViT, have a longer running time than methods that do not perform reconstruction. Both FQ-ViT and RepQ-ViT do not use reconstruction; however, FQ-ViT requires 1,000 images for calibration, thus consuming more time than RepQ-ViT, which uses only 32 images. However, these differences are trivial when compared to the substantial number of GPU hours produced by quantization-aware training methods. Since post-training quantization is performed only once offline, these minute differences are negligible.

E. Ablation Study on Hybrid Reconstruction

We performed an ablation study to assess the impact of utilizing the optimal selection of scaling factors, granularity, and quantization scheme within the context of hybrid reconstruction error minimization. Furthermore, every functional component in hybrid vision transformers tackles one of the four challenges that arise. Conducting an ablation study enables us to assess the degree of mitigation empirically.

Table IV provides a summary of the ablation study results for various sizes and types of hybrid vision transformer architectures, where the results demonstrate that all the components enhance the accuracy of quantized hybrid ViTs.

When only optimizing the scaling factor with hybrid reconstruction error minimization, it does not yield significant performance improvements compared to PTQ4ViT (baseline). However, optimizing not only the scaling factors but also the granularity and scheme based on the bridge block leads to synergistic effects in general. As a result, combining all of them together achieves significant accuracy improvements. In contrast, excluding the optimization of granularity significantly decreases the accuracy, highlighting highly dynamic activation ranges in lightweight hybrid ViTs as the main cause of the accuracy drop.

VI. IMPLICATIONS AND RECOMMENDATIONS FOR IOT

Quantization method significantly contributes to the IoT domain by enabling efficient computation and communication, which are essential for deploying artificial intelligence and machine learning models on IoT devices. We describe a roadmap for integrating quantization in IoT applications, system software support, and hardware design.

Enhancing IoT Applications through Efficient Federated Learning FedQNN [2] and QuAsyncFL [3] showcase how quantization facilitates federated learning in IoT by reducing the model's bitwidth, thus lowering the computational and communication overhead. This enables IoT devices to participate in federated learning networks more effectively, allowing for distributed, privacy-preserving machine learning without the need for high bandwidth or powerful computational resources. By adopting low-bitwidth neural network quantization and asynchronous federated learning approaches, IoT applications can achieve smarter data processing and decision-making capabilities, improving areas such as smart agriculture, healthcare monitoring, and urban traffic management.

IoT Hardware Design support: The implementation of efficient neural networks within the IoT domain necessitates a reevaluation of hardware design for IoT devices. For this reason, hardware tailored for efficient neural network inference on IoT devices has been developed [52], [53]. These specialized hardware solutions for the IoT aim to reduce design complexity and enhance power efficiency by supporting 8-bit operations. Achieving this operational support requires the use of quantization techniques, which are essential and can also leverage the quantization methods proposed in this research.

VII. CONCLUSION

We addressed the problem of democratizing vision transformers on resource-constrained devices by proposing a method for minimizing quantization errors in hybrid vision transformers. The proposed method, Q-HyViT, identified the four challenges of applying post-training quantization (PTQ) to hybrid vision transformers and proposed a unified method to mitigate errors in PTQ. Q-HyViT achieved this by selecting optimal scale factors, granularity, and scheme for both bridge and non-bridge layers based on hybrid reconstruction error minimization from a loss degradation perspective. We demonstrated the effectiveness of Q-HyViT by conducting extensive experiments comparing it with existing several open-source algorithms, EasyQuant, FQ-ViT, PTQ4ViT, and RepQ-ViT on the same hybrid vision transformers. The results demonstrated that Q-HyViT outperforms existing methods by a significant margin and achieved state-of-the-art accuracy on hybrid vision transformers in a fully quantized manner, including non-linear operations such as softmax and diverse normalization. Finally, we contributed to the field of artificial intelligence by identifying the four unique challenges of quantizing hybrid vision transformers and proposing an effective solution for minimizing quantization error.

REFERENCES

- [1] S. Chen, L. Li, G. Wang, M. Pang, and C. Shen, "Federated learning with heterogeneous quantization bit allocation and aggregation for internet of things," *IEEE Internet of Things Journal*, 2023.
- [2] Y. Ji and L. Chen, "Fedqnn: A computation-communication-efficient federated learning framework for iot with low-bitwidth neural network quantization," *IEEE Internet of Things Journal*, vol. 10, no. 3, pp. 2494–2507, 2022.
- [3] Y. Liu, P. Huang, F. Yang, K. Huang, and L. Shu, "Quasyncl: Asynchronous federated learning with quantization for cloud-edge-terminal collaboration enabled aiot," *IEEE Internet of Things Journal*, 2023.

- [4] K. Han, Y. Wang, H. Chen, X. Chen, J. Guo, Z. Liu, Y. Tang, A. Xiao, C. Xu, Y. Xu *et al.*, "A survey on vision transformer," *IEEE transactions on pattern analysis and machine intelligence*, vol. 45, no. 1, pp. 87–110, 2022.
- [5] S. Khan, M. Naseer, M. Hayat, S. W. Zamir, F. S. Khan, and M. Shah, "Transformers in vision: A survey," *ACM computing surveys (CSUR)*, vol. 54, no. 10s, pp. 1–41, 2022.
- [6] S. Mehta and M. Rastegari, "Mobilevit: light-weight, general-purpose, and mobile-friendly vision transformer," *arXiv preprint arXiv:2110.02178*, 2021.
- [7] —, "Separable self-attention for mobile vision transformers," *Transactions on Machine Learning Research*, 2022.
- [8] R. Krishnamoorthi, "Quantizing deep convolutional networks for efficient inference: A whitepaper," *arXiv preprint arXiv:1806.08342*, 2018.
- [9] S. K. Esser, J. L. McKinstry, D. Bablani, R. Appuswamy, and D. S. Modha, "Learned step size quantization," in *8th International Conference on Learning Representations, ICLR 2020, Addis Ababa, Ethiopia, April 26-30, 2020*. OpenReview.net, 2020, pp. 1–12.
- [10] J. Choi, Z. Wang, S. Venkataramani, P. I.-J. Chuang, V. Srinivasan, and K. Gopalakrishnan, "Pact: Parameterized clipping activation for quantized neural networks," in *6th International Conference on Learning Representations, ICLR 2018, Vancouver, BC, Canada, April 30 - May 3, 2018, Conference Track Proceedings*. OpenReview.net, 2018. [Online]. Available: <https://openreview.net/forum?id=ryQu7f-RZ>
- [11] D. Zhang, J. Yang, D. Ye, and G. Hua, "Lq-nets: Learned quantization for highly accurate and compact deep neural networks," in *Proceedings of the European conference on computer vision (ECCV)*, 2018, pp. 365–382.
- [12] S. Jung, C. Son, S. Lee, J. Son, J.-J. Han, Y. Kwak, S. J. Hwang, and C. Choi, "Learning to quantize deep networks by optimizing quantization intervals with task loss," in *Proceedings of the IEEE/CVF Conference on Computer Vision and Pattern Recognition*, 2019, pp. 4350–4359.
- [13] S. Zhou, Y. Wu, Z. Ni, X. Zhou, H. Wen, and Y. Zou, "Dorefa-net: Training low bitwidth convolutional neural networks with low bitwidth gradients," *arXiv preprint arXiv:1606.06160*, 2016.
- [14] B. Jacob, S. Kligys, B. Chen, M. Zhu, M. Tang, A. Howard, H. Adam, and D. Kalenichenko, "Quantization and training of neural networks for efficient integer-arithmetic-only inference," in *Proceedings of the IEEE Conference on Computer Vision and Pattern Recognition*, 2018, pp. 2704–2713.
- [15] S. Han, H. Mao, and W. J. Dally, "Deep compression: Compressing deep neural network with pruning, trained quantization and Huffman coding," in *4th International Conference on Learning Representations, ICLR 2016, San Juan, Puerto Rico, May 2-4, 2016, Conference Track Proceedings*, Y. Bengio and Y. LeCun, Eds., 2016. [Online]. Available: <http://arxiv.org/abs/1510.00149>
- [16] Z. Jiang, A. Jain, A. Liu, J. Fromm, C. Ma, T. Chen, and L. Ceze, "Automated backend-aware post-training quantization," *arXiv preprint arXiv:2103.14949*, 2021.
- [17] R. Banner, Y. Nahshan, and D. Soudry, "Post training 4-bit quantization of convolutional networks for rapid-deployment," in *Advances in Neural Information Processing Systems*, H. Wallach, H. Larochelle, A. Beygelzimer, F. d'Alché-Buc, E. Fox, and R. Garnett, Eds., vol. 32. Curran Associates, Inc., 2019.
- [18] Y. Choukroun, E. Kravchik, F. Yang, and P. Kisilev, "Low-bit quantization of neural networks for efficient inference," in *ICCV Workshops*, 2019, pp. 3009–3018.
- [19] R. Zhao, Y. Hu, J. Dotzel, C. De Sa, and Z. Zhang, "Improving neural network quantization without retraining using outlier channel splitting," in *International conference on machine learning*. PMLR, 2019, pp. 7543–7552.
- [20] J. H. Lee, S. Ha, S. Choi, W.-J. Lee, and S. Lee, "Quantization for rapid deployment of deep neural networks," *arXiv preprint arXiv:1810.05488*, 2018.
- [21] A. Goncharenko, A. Denisov, S. Alyamkin, and E. Terentev, "Fast adjustable threshold for uniform neural network quantization," *International Journal of Computer and Information Engineering*, vol. 13, no. 9, pp. 495–499, 2019.
- [22] S. Migacz, "8-bit inference with tensorrt," in *GPU technology conference*, vol. 2, no. 4, 2017, p. 5.
- [23] H. Wu, P. Judd, X. Zhang, M. Isaev, and P. Micikevicius, "Integer quantization for deep learning inference: Principles and empirical evaluation," *arXiv preprint arXiv:2004.09602*, 2020.
- [24] A. Dosovitskiy, L. Beyer, A. Kolesnikov, D. Weissenborn, X. Zhai, T. Unterthiner, M. Dehghani, M. Minderer, G. Heigold, S. Gelly *et al.*,

- “An image is worth 16x16 words: Transformers for image recognition at scale,” *arXiv preprint arXiv:2010.11929*, 2020.
- [25] H. Touvron, M. Cord, M. Douze, F. Massa, A. Sablayrolles, and H. Jégou, “Training data-efficient image transformers & distillation through attention,” in *International conference on machine learning*. PMLR, 2021, pp. 10 347–10 357.
- [26] Z. Liu, Y. Lin, Y. Cao, H. Hu, Y. Wei, Z. Zhang, S. Lin, and B. Guo, “Swin transformer: Hierarchical vision transformer using shifted windows,” in *Proceedings of the IEEE/CVF international conference on computer vision*, 2021, pp. 10 012–10 022.
- [27] D. Wu, Q. Tang, Y. Zhao, M. Zhang, Y. Fu, and D. Zhang, “Easyquant: Post-training quantization via scale optimization,” *arXiv preprint arXiv:2006.16669*, 2020.
- [28] Y. Lin, T. Zhang, P. Sun, Z. Li, and S. Zhou, “Fq-vit: Post-training quantization for fully quantized vision transformer,” in *Proceedings of the Thirty-First International Joint Conference on Artificial Intelligence, IJCAI-22*, 2022, pp. 1173–1179.
- [29] Z. Yuan, C. Xue, Y. Chen, Q. Wu, and G. Sun, “Ptq4vit: Post-training quantization for vision transformers with twin uniform quantization,” in *European Conference on Computer Vision*. Springer, 2022, pp. 191–207.
- [30] Z. Li, J. Xiao, L. Yang, and Q. Gu, “Repq-vit: Scale reparameterization for post-training quantization of vision transformers,” in *Proceedings of the IEEE/CVF International Conference on Computer Vision*, 2023, pp. 17 227–17 236.
- [31] Y. Chen, X. Dai, D. Chen, M. Liu, X. Dong, L. Yuan, and Z. Liu, “Mobile-former: Bridging mobilenet and transformer,” in *Proceedings of the IEEE/CVF Conference on Computer Vision and Pattern Recognition*, 2022, pp. 5270–5279.
- [32] Y. Li, G. Yuan, Y. Wen, J. Hu, G. Evangelidis, S. Tulyakov, Y. Wang, and J. Ren, “Efficientformer: Vision transformers at mobilenet speed,” *Advances in Neural Information Processing Systems*, vol. 35, pp. 12 934–12 949, 2022.
- [33] Y. Li, J. Hu, Y. Wen, G. Evangelidis, K. Salahi, Y. Wang, S. Tulyakov, and J. Ren, “Rethinking vision transformers for mobilenet size and speed,” in *Proceedings of the IEEE international conference on computer vision*, 2023.
- [34] F. Chollet, “Xception: Deep learning with depthwise separable convolutions,” in *Proceedings of the IEEE conference on computer vision and pattern recognition*, 2017, pp. 1251–1258.
- [35] A. G. Howard, M. Zhu, B. Chen, D. Kalenichenko, W. Wang, T. Weyand, M. Andreetto, and H. Adam, “Mobilenets: Efficient convolutional neural networks for mobile vision applications,” *arXiv preprint arXiv:1704.04861*, 2017.
- [36] M. Sandler, A. Howard, M. Zhu, A. Zhmoginov, and L.-C. Chen, “Mobilenetv2: Inverted residuals and linear bottlenecks,” in *Proceedings of the IEEE conference on computer vision and pattern recognition*, 2018, pp. 4510–4520.
- [37] A. Howard, M. Sandler, G. Chu, L.-C. Chen, B. Chen, M. Tan, W. Wang, Y. Zhu, R. Pang, V. Vasudevan *et al.*, “Searching for mobilenetv3,” in *Proceedings of the IEEE/CVF international conference on computer vision*, 2019, pp. 1314–1324.
- [38] N. Ma, X. Zhang, H.-T. Zheng, and J. Sun, “Shufflenet v2: Practical guidelines for efficient cnn architecture design,” in *Proceedings of the European conference on computer vision (ECCV)*, 2018, pp. 116–131.
- [39] M. Tan, B. Chen, R. Pang, V. Vasudevan, M. Sandler, A. Howard, and Q. V. Le, “Mnasnet: Platform-aware neural architecture search for mobile,” in *Proceedings of the IEEE/CVF conference on computer vision and pattern recognition*, 2019, pp. 2820–2828.
- [40] M. Nagel, M. v. Baalen, T. Blankevoort, and M. Welling, “Data-free quantization through weight equalization and bias correction,” in *Proceedings of the IEEE/CVF International Conference on Computer Vision*, 2019, pp. 1325–1334.
- [41] E. Meller, A. Finkelstein, U. Almog, and M. Grobman, “Same, same but different: Recovering neural network quantization error through weight factorization,” in *Proceedings of the 36th International Conference on Machine Learning*, ser. Proceedings of Machine Learning Research, K. Chaudhuri and R. Salakhutdinov, Eds., vol. 97. PMLR, 09–15 Jun 2019, pp. 4486–4495.
- [42] M. Nagel, R. A. Amjad, M. Van Baalen, C. Louizos, and T. Blankevoort, “Up or down? adaptive rounding for post-training quantization,” in *International Conference on Machine Learning*. PMLR, 2020, pp. 7197–7206.
- [43] Y. Li, R. Gong, X. Tan, Y. Yang, P. Hu, Q. Zhang, F. Yu, W. Wang, and S. Gu, “Brecq: Pushing the limit of post-training quantization by block reconstruction,” *arXiv preprint arXiv:2102.05426*, 2021.
- [44] I. Hubara, Y. Nahshan, Y. Hanani, R. Banner, and D. Soudry, “Accurate post training quantization with small calibration sets,” in *International Conference on Machine Learning*. PMLR, 2021, pp. 4466–4475.
- [45] X. Wei, R. Gong, Y. Li, X. Liu, and F. Yu, “Qdrop: randomly dropping quantization for extremely low-bit post-training quantization,” *arXiv preprint arXiv:2203.05740*, 2022.
- [46] C. Wang, D. Zheng, Y. Liu, and L. Li, “Leveraging inter-layer dependency for post-training quantization,” in *Advances in Neural Information Processing Systems*.
- [47] Z. Liu, Y. Wang, K. Han, W. Zhang, S. Ma, and W. Gao, “Post-training quantization for vision transformer,” *Advances in Neural Information Processing Systems*, vol. 34, pp. 28 092–28 103, 2021.
- [48] Y. Ding, H. Qin, Q. Yan, Z. Chai, J. Liu, X. Wei, and X. Liu, “Towards accurate post-training quantization for vision transformer,” in *Proceedings of the 30th ACM International Conference on Multimedia*, 2022, pp. 5380–5388.
- [49] Y. Liu, H. Yang, Z. Dong, K. Keutzer, L. Du, and S. Zhang, “Noisyquant: Noisy bias-enhanced post-training activation quantization for vision transformers,” in *Proceedings of the IEEE/CVF Conference on Computer Vision and Pattern Recognition*, 2023, pp. 20 321–20 330.
- [50] R. Li, Y. Wang, F. Liang, H. Qin, J. Yan, and R. Fan, “Fully quantized network for object detection,” in *Proceedings of the IEEE/CVF conference on computer vision and pattern recognition*, 2019, pp. 2810–2819.
- [51] B. Jacob, S. Kligys, B. Chen, M. Zhu, M. Tang, A. Howard, H. Adam, and D. Kalenichenko, “Quantization and training of neural networks for efficient integer-arithmetic-only inference,” in *Proceedings of the IEEE Conference on Computer Vision and Pattern Recognition*, 2018, pp. 2704–2713.
- [52] D. Yang and Z. Luo, “A parallel processing cnn accelerator on embedded devices based on optimized mobilenet,” *IEEE Internet of Things Journal*, 2023.
- [53] E. Russo, M. Palesi, S. Monteleone, D. Patti, A. Mineo, G. Ascia, and V. Catania, “Dnn model compression for iot domain-specific hardware accelerators,” *IEEE Internet of Things Journal*, vol. 9, no. 9, pp. 6650–6662, 2021.



aware mobile computing and deep learning compilers.



neural processing units, compiler, deep learning, and embedded systems.

Jemin Lee received his B.S. and Ph.D. degrees in computer science and engineering from Chungnam National University in 2011 and 2017, respectively. He is currently a senior researcher at the Electronics and Telecommunications Research Institute (ETRI). Since 2023, he has also served as an assistant professor in the AI Department at the University of Science and Technology (UST). Previously, he was a postdoctoral researcher at the Korea Advanced Institute of Science and Technology (KAIST) from 2017 to 2018. His research interests include energy-

Yongin Kwon received the B.Sc. degree in electrical and electronic engineering from the Korea Advanced Institute of Science and Technology, South Korea, in 2008, and M.S. and Ph.D. degrees in electrical and computer engineering from Seoul National University, South Korea, in 2010 and 2015, respectively. From 2015 to 2019, he worked at Samsung Electronics as a Staff Software Engineer. He has been with Electronics and Telecommunications Research Institute (ETRI) since 2019, where he is currently a Senior Researcher. His research interests include



Sihyeong Park received the B.S., M.S., and Ph.D. degrees in computer science and engineering from Chungnam National University, in 2014, 2016, and 2021, respectively. He is a senior researcher at the Korea Electronics Technology Institute (KETI). His research interests include multi-core embedded systems and real-time systems.



Misun Yu received the M.S. degree from the Department of Computer Science and Engineering at Pohang University of Science and Technology, Republic of Korea. She is a principal researcher at the Electronics and Communications Research Institute (ETRI), Daejeon, Rep. of Korea. Her main research interests include concurrent program analysis, software testing, deep learning, and embedded systems.



Jeman Park received his B.S., M.S., and Ph.D. degrees in electronics and computer engineering in Hanyang University, Republic of Korea, in 2004, 2006, and 2014, respectively. Since 2019, he has been with Electronics and Telecommunications Research Institute, Daejeon, Republic of Korea, where he is now a senior researcher. His main research interests are computer network, edge computing, and AI compiler.



Hwanjun Song is an assistant professor in the Department of Industrial and Systems Engineering at KAIST. Previously, he was a Research Scientist at AWS AI Labs in 2023 and at NAVER AI Lab in 2021–2022, and Research Intern at Google Research in 2020. He earned his Ph.D. degree in the Graduate School of Data Science from KAIST in 2021. He is interested in designing advanced methodologies to handle data scale and quality issues, which are two main real-world challenges for AI. He was sponsored by Microsoft through Azure for Research from 2016 to 2018, and received the Qualcomm Innovation Award in 2019.